

Provided for non-commercial research and education use.
Not for reproduction, distribution or commercial use.



This article appeared in a journal published by Elsevier. The attached copy is furnished to the author for internal non-commercial research and education use, including for instruction at the authors institution and sharing with colleagues.

Other uses, including reproduction and distribution, or selling or licensing copies, or posting to personal, institutional or third party websites are prohibited.

In most cases authors are permitted to post their version of the article (e.g. in Word or Tex form) to their personal website or institutional repository. Authors requiring further information regarding Elsevier's archiving and manuscript policies are encouraged to visit:

<http://www.elsevier.com/authorsrights>



Fabrication of nano Delafossite $\text{LiCo}_{0.5}\text{Fe}_{0.5}\text{O}_2$ as the new adsorbent in efficient removal of reactive blue 5 from aqueous solutions

Iman Khosravi^{a,*}, Mohammad Yazdanbakhsh^b, Melika Eftekhari^a, Zohreh Haddadi^b

^a Department of Chemistry, Qeshm Branch, Islamic Azad University, Qeshm, Iran

^b Department of Chemistry, Faculty of Sciences, Ferdowsi University of Mashhad, Mashhad 917791436, Iran

ARTICLE INFO

Article history:

Received 30 July 2012

Received in revised form 14 January 2013

Accepted 17 February 2013

Available online 28 February 2013

Keywords:

A. Nanostructures

A. Inorganic compounds

B. Chemical synthesis

B. Sol–gel chemistry

C. X-ray diffraction

ABSTRACT

In this paper, nanoparticles of delafossite-type $\text{LiCo}_{0.5}\text{Fe}_{0.5}\text{O}_2$ were prepared by sol–gel method in the presence of maleic acid as a chelating agent. The nanoparticles were characterized using differential thermal analysis, X-ray powder diffraction, Fourier infrared spectroscopy, transmission electron microscope, scanning electron microscopy and scanning tunneling microscopy. The nanoparticles showed the excellent adsorption properties towards reactive dye, reactive blue 5 (RB5). The adsorption studies were carried out at different pH values, various adsorbent dosages and contact time in a batch experiments. The kinetic studies indicate that the removal process obeys the second-order kinetic equation. Also, the isotherm evaluations reveal that the adsorption of RB5 by the nanoparticles follows the Freundlich model.

© 2013 Elsevier Ltd. All rights reserved.

1. Introduction

Dyes are important water pollutants in effluents of textile, paper, printing, and leather industries. The presence of dyes in water reduces light penetration and hinders photosynthesis in aquatic plants. Some dyes and their degradation products in surface water are reported to be highly carcinogenic [1]. It is, therefore, essential to treat the dye effluents prior to their discharge into the receiving water. Dyes are organic compounds consisting of two main groups of compounds, chromophores and auxochromes [2]. Dyes are classified according to the chemical structure and type of application.

Many processes are employed to remove dye molecules from colored effluents; in general, treatment methods can be divided into three categories, (1) physical methods, such as adsorption [3], and membrane filtration [4], (2) chemical methods, such as ionic exchange [5], chemical oxidation [6] and ozonation [7] and (3) biological degradation [8].

Adsorption techniques for wastewater treatment have become more popular in recent years because of their efficiency in the removal of pollutants which are stable in biological degradation process. Adsorption can produce high quality water while also being a process that is economically feasible [9].

The Delafossite-type oxides generally formulated as ABO_2 (the A cation like Li^+ is coordinated to six oxygen ions and the B cation like Fe^{3+} or Co^{3+} is located in distorted BO_6 octahedral sharing edges) could be considered as an adsorbent/catalyst material for the removal of dyes [10].

Though, several articles have investigated the effectiveness of spinel [11,12] and perovskite [13] oxides as catalysts for removal of water-soluble dyes, to the best of our knowledge, the confirmation and optimization of the efficiency of the delafossite oxides catalysts and the degradation pathway for the removal of reactive dyes from aqueous solution have received little attention in the literature.

This study has investigated the efficiency of delafossite-type oxide nanoparticles $\text{LiCo}_{0.5}\text{Fe}_{0.5}\text{O}_2$ as an adsorbent for removal of reactive blue 5 (RB5) from an aqueous solution. The adsorption studies were carried out at different pH values, various adsorbent dosages and contact time in a batch experiments. Two kinetic models were also analyzed for the removal of RB5 on $\text{LiCo}_{0.5}\text{Fe}_{0.5}\text{O}_2$ nanoparticles. Furthermore, preparation of $\text{LiCo}_{0.5}\text{Fe}_{0.5}\text{O}_2$ nanoparticles via sol–gel method and its characterization by different techniques such as DTA, Far-IR, XRD, STM, SEM and TEM have been reported.

2. Materials and methods

2.1. Reagents

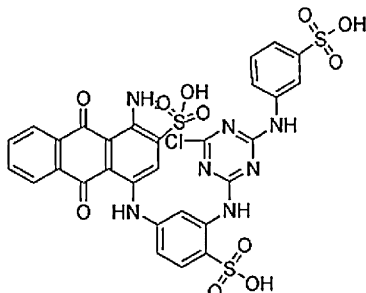
LiNO_3 (99.9% purity), $\text{Co}(\text{NO}_3)_2 \cdot 6\text{H}_2\text{O}$ (99.9% purity), $\text{Fe}(\text{NO}_3)_3 \cdot 9\text{H}_2\text{O}$ (99.9% purity) were obtained from Merck, Germany;

* Corresponding author. Tel.: +98 7635263309; fax: +98 7635263598.

E-mail address: khosraviiman@yahoo.com (I. Khosravi).

Table 1

Molecular structure of the studied dye.

Dye	Name	Structure	λ_{\max} (nm)	M_w
RB5	Reactive blue 5		599	774.16 (g mol ⁻¹)

maleic acid (99.5% purity) was purchased from Aldrich, USA. The commercial color index (CI) reactive dye (RB5) was generously provided by Arzoo Textile Mills, Faisalabad, Pakistan which was used without further purification (Table 1). All the reagents were of analytical grade and thus used as received.

2.2. Adsorbent preparation

A stoichiometric amount of Li:Co:Fe nitrate salts with the cationic ratio of 1:0.5:0.5 respectively, were dissolved in distilled water and mixed well with an aqueous solution of maleic acid (the ratio of maleic acid to total metal ions is 2:1). Maleic acid was used as a chelating agent in making a gel. The resultant solution was then evaporated at 80 °C with magnetic stirring for 12 h. The gel precursors were decomposed at 400 °C for 1 h in air to eliminate organic contents. The powders were heated to 600 °C to obtain the single phase LiCo_{0.5}Fe_{0.5}O₂ powders.

Several techniques were employed to analyze and validate the synthesized powder. The nanoparticles were characterized by XRD employing a scanning rate of 0.02 s⁻¹ in a 2 θ range from 0° to 70°, using an X pert, 200, Philips, equipped with CuK α radiation and the data were analyzed using JCPDS standards.

The morphology and dimension of the nanoparticles were observed by LEO 912 AB transmission electron microscope (TEM) using an accelerating voltage of 120 kV, and the morphology of the particles was investigated using LEO 1450 VP (V = 30 kV) scanning electron microscopy (SEM) and SS1 STM, scanning tunneling microscopy (STM). All images were recorded in the constant-current mode at room temperature using a Remanium tip with a bias voltage of around 2 V in atmosphere.

The thermal behavior of the precursor was studied by differential thermal analysis (DTA) in air at a heating rate of 10 °C min⁻¹ using NETZSCH.

The infrared spectrum (FTIR) was recorded in the 250–4000 cm⁻¹ range (KBr pellets) on thermo Nicolet Nexus 870 FTIR spectrometer equipped with DTGS polyethylene detector and solid subtract beam splitter IR spectrometer.

The zeta potentials of nanoparticles were measured at different pH using a CAD, zeta compact analyzer.

2.3. Dye removal experiments

The synthetic dye solution was distributed into different flasks (1 L capacity) and pH was adjusted with the help of pH meter (Metrohm 620). The initial pH of the sample was set by using dilute sodium hydroxide (1 M) or hydrochloric acid (1 M).

The initial dye concentration in each sample was 50 mg l⁻¹ after adding LiCo_{0.5}Fe_{0.5}O₂ in 50 ml of the sample. The removal pollution experiments were conducted at 25 °C and the pH was varied from 1 to 11.

Each experiment was conducted for 10 min and samples were drawn at time intervals of 1, 3, 5, 7, and 10 min for measuring the dye adsorption. The absorbance of the solution at 599 nm (UNICO 2800) with time was measured to monitor the RB5 concentration.

3. Results and discussion

3.1. Thermal analysis

Fig. 1 shows DTA of the gel precursor prepared by sol gel method. The large endothermic peak at 120 °C corresponds to the removal of superficial and structural waters in the gel precursor. Three exothermic peaks around 200–300 °C are due to the combustion of maleic acid and nitrate ions. It seems that maleic acid acts as a fuel in the pyrolysis of the gel precursors and accelerating the decomposition of nitrate ions [14]. The exothermic peak at 500 °C in the DTA curve corresponds to the crystallization of the LiCo_{0.5}Fe_{0.5}O₂ phase.

3.2. X-ray diffraction studies

Fig. 2 shows the XRD powder patterns using CuK α radiation from the delafossite-type LiCo_{0.5}Fe_{0.5}O₂ nanoparticles. The analysis of the diffraction pattern using (0 0 3), (1 0 1), (0 0 6), (1 0 2), (1 0 4), (0 1 5), (1 0 7), (1 1 0), and (1 1 3) reflection planes confirms the formation of rhombohedral delafossite structure with (R3m) space group of the LiCo_{0.5}Fe_{0.5}O₂ [15].

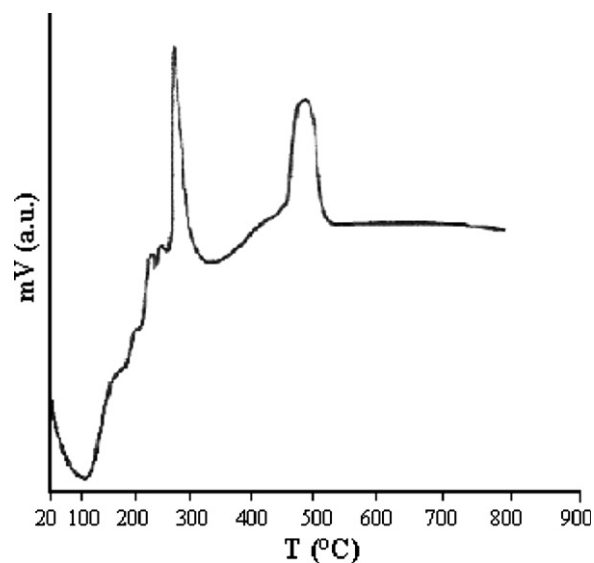


Fig. 1. DTA curve of the LiCo_{0.5}Fe_{0.5}O₂ precursors obtained by the maleic acid assisted sol-gel method.

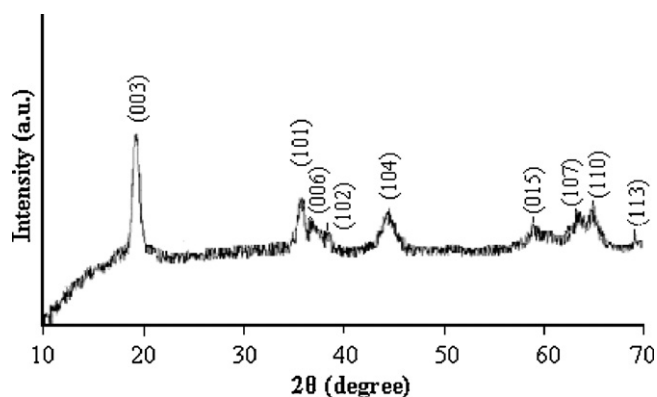


Fig. 2. XRD patterns of the $\text{LiCo}_{0.5}\text{Fe}_{0.5}\text{O}_2$ powders sintered at $600\text{ }^\circ\text{C}$.

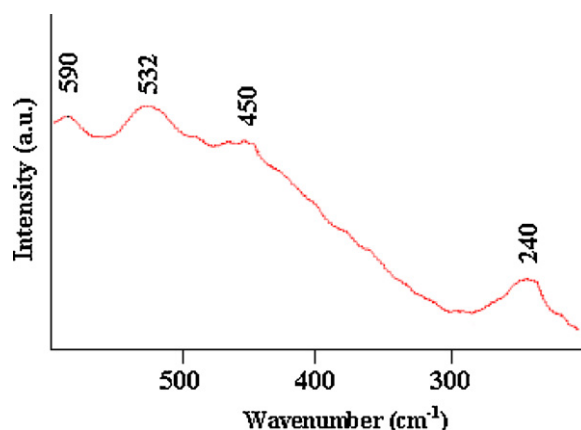


Fig. 3. Far-IR spectrum of $\text{LiCo}_{0.5}\text{Fe}_{0.5}\text{O}_2$.

No secondary phase was detected in the XRD pattern which ensures the phase purity of the final products. The crystallite sizes were calculated using the XRD peak broadening of the (0 0 3) peak using the Scherrer's formula (Eq. (1)):

$$D_{hkl} = \frac{0.9\lambda}{\beta_{hkl}\cos\theta_{hkl}} \quad (1)$$

where D_{hkl} is the particle size perpendicular to the normal line of (hkl) plane, β_{hkl} is the full width at half maximum, θ_{hkl} is the Bragg angle of (hkl) peak, and λ is the wavelength of X-ray. The crystallite particle size of nanoparticles calcinated at $600\text{ }^\circ\text{C}$ is about 44 nm.

3.3. IR spectra of annealed particles

IR scattering spectra of $\text{LiCo}_{0.5}\text{Fe}_{0.5}\text{O}_2$ oxide confirm the X-ray pattern. According to the group theoretical analysis, the vibrational spectra of the LiMO_2 compounds with $R3m$ space group yield four infrared active modes ($2A_{2u} + 2E_u$). Considering the localized molecular approach, the stretching modes of MO_6 octahedral occur in the high-frequency region ($450\text{--}620\text{ cm}^{-1}$) while the stretching mode of a LiO_6 octahedron is observed in the far IR region at $230\text{--}270\text{ cm}^{-1}$ [16].

Fig. 3 shows the far IR spectrum of the nanoparticles. The vibration mode of LiO_6 unit, observed at 240 cm^{-1} and the high frequency band located at 590 cm^{-1} is attributed to the asymmetric stretching mode of CoO_6 group whereas the low

frequency bands at 450 cm^{-1} and 532 cm^{-1} are assigned to the bending modes of O–M–O chemical bonds [17].

3.4. Microscopic analyses

The size of Delafossite particles was evaluated and conformed by TEM. Fig. 4 shows representative TEM image of $\text{LiCo}_{0.5}\text{Fe}_{0.5}\text{O}_2$. The image of the sample which calcinated at $600\text{ }^\circ\text{C}$ consists of particles ranging in size of about 44 nm. As the TEM images show, the morphology of nanoparticles is homogeneous [18].

Scanning electron microscopy (SEM) of Delafossite oxide $\text{LiCo}_{0.5}\text{Fe}_{0.5}\text{O}_2$ prepared by the sol–gel method and calcinated at $600\text{ }^\circ\text{C}$ is shown in Fig. 5. Based on the SEM image, porosity of the surface is evident and it seems that the particles have not grown with uniform size. The surface looks rough and nearly fully covered with the particles grown on it. Further, it can also be seen from the SEM result that in addition to the larger particles, the surface contains also rather smaller particles as down to 30 nm or less. However, appearance of bigger particles on the surface looks to be dominant. The aggregation of the smaller particles (the nm range) may result in bigger $\text{LiCo}_{0.5}\text{Fe}_{0.5}\text{O}_2$ particles on the surface.

Fig. 6 shows the scanning tunneling microscopy (STM) images ($500\text{ nm} \times 500\text{ nm}$) of $\text{LiCo}_{0.5}\text{Fe}_{0.5}\text{O}_2$ nanoparticles which can be used to determine the particles size and height. In Fig. 6(a), the bright spots are higher than the dark ones and particles distribution on the surface is mapped obviously. In Fig. 6(b), four particles were selected for quantitative measurements and results

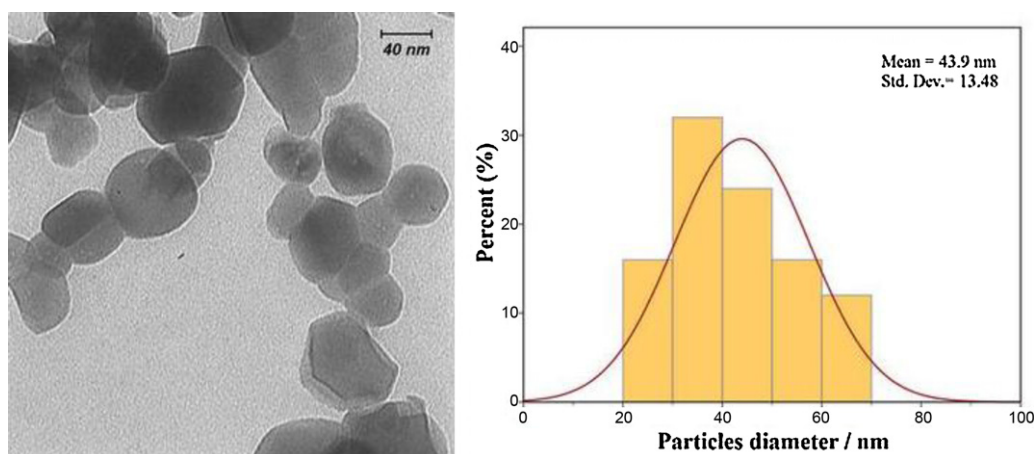


Fig. 4. TEM micrograph and calculated histogram of the $\text{LiCo}_{0.5}\text{Fe}_{0.5}\text{O}_2$ nanoparticles obtained at $600\text{ }^\circ\text{C}$.

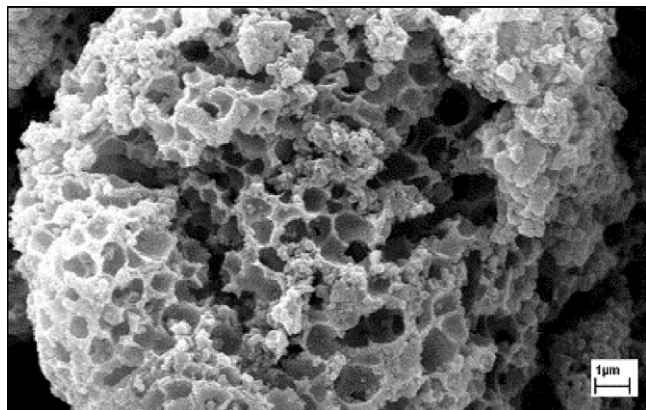


Fig. 5. SEM image of $\text{LiCo}_{0.5}\text{Fe}_{0.5}\text{O}_2$ nanoparticles.

showed that their average size and height were obtained around 45 nm and 7 nm, respectively.

3.5. Zeta potentials analysis

The zeta potential, which is the overall charge a particle acquires in a specific medium, is a good indicator of the stability of the colloidal system. The zeta potential of colloidal dispersions of $\text{LiCo}_{0.5}\text{Fe}_{0.5}\text{O}_2$ in water (Fig. 7) was measured. The isoelectric point (IEP) was found to be at $\text{pH} = 6.3$. The colloidal system is the least

stable at this point due to the absence of particle surface charges. The zeta potential of the suspensions of $\text{LiCo}_{0.5}\text{Fe}_{0.5}\text{O}_2$ nanoparticles in water reaches as high as 40 mV at acidic pH.

3.6. Adsorption studies

The efficiency of prepared $\text{LiCo}_{0.5}\text{Fe}_{0.5}\text{O}_2$ nanoparticles was investigated as an adsorbent for the removal of RB5 from liquid solutions. The removal pollution experiments were conducted at 25°C and were carried out for different pH values, contact time and adsorbent doses.

3.6.1. The effect of pH

The pH of the dye solution plays an important role in the whole adsorption process. To determine the optimum pH, the pH value was changed from 1 to 11 with fixed initial concentration of dye (50 mg l^{-1}) and contact time (10 min). Fig. 8 shows the percentage of removal rate of RB5 by $\text{LiCo}_{0.5}\text{Fe}_{0.5}\text{O}_2$ nanoparticles depends strongly on pH.

The percentage of removal rate is defined as (Eq. (2)):

$$\text{Removal rate } \% = \frac{C_0 - C(t)}{C_0} \times 100 \quad (2)$$

where C_0 and $C(t)$ are the initial concentration and concentration of RB5 at time t , respectively [19]. At $\text{pH} = 1$, the removal of RB5 above 97% is achieved. This pH is below the isoelectric point and hence adsorbent surface is positive charge and anion adsorption occurs. Therefore, this pH has been selected for our next experiments.

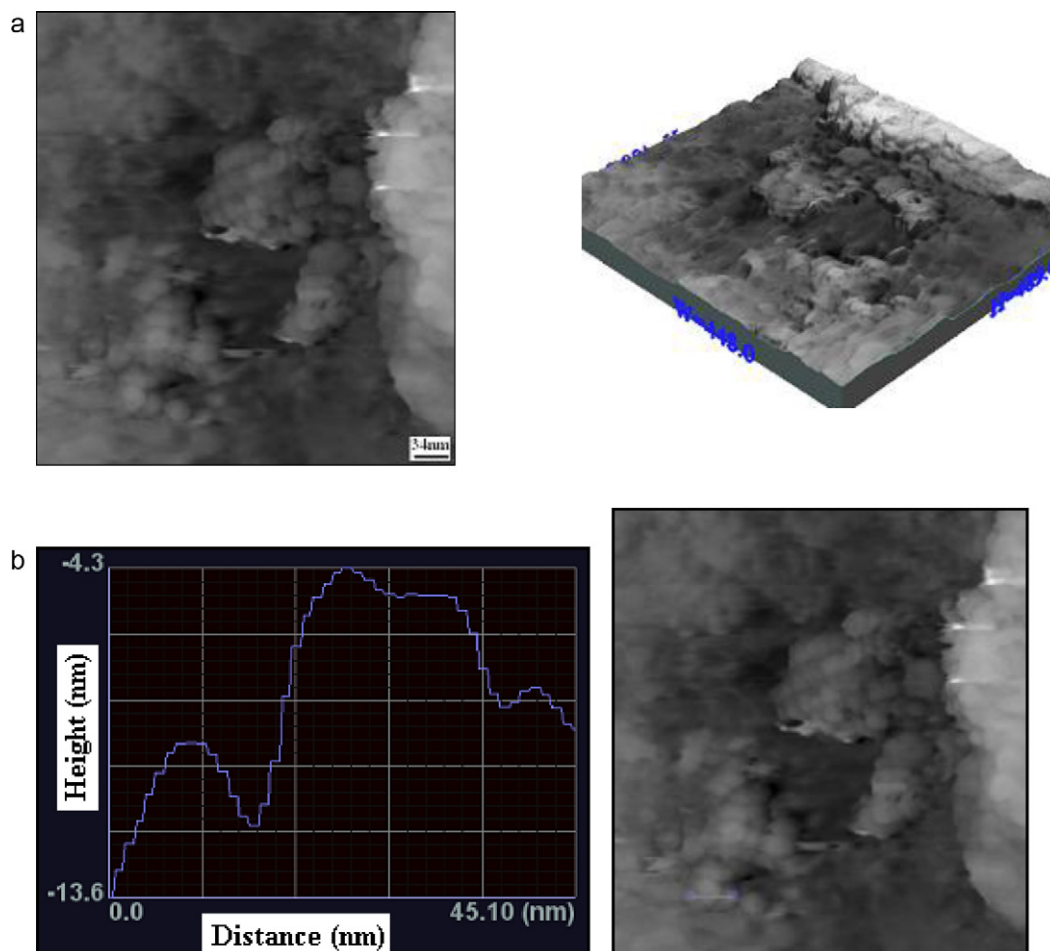


Fig. 6. (a) STM images of $\text{LiCo}_{0.5}\text{Fe}_{0.5}\text{O}_2$ for the area of $500\text{ nm} \times 500\text{ nm}$. (b) Height profile along the white line.

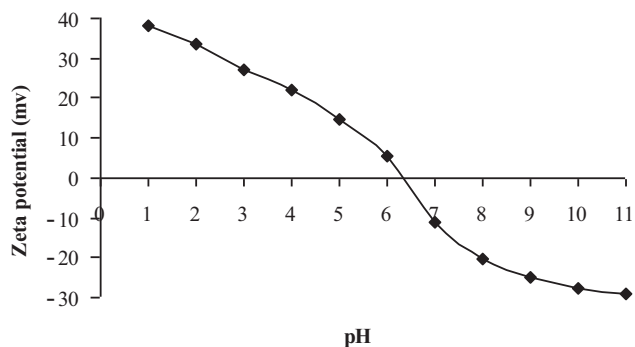


Fig. 7. Zeta potentials of the $\text{LiCo}_{0.5}\text{Fe}_{0.5}\text{O}_2$ nanoparticles at different pH.

3.6.2. The effect of contact time

The effect of contact time on the removal of RB5 by $\text{LiCo}_{0.5}\text{Fe}_{0.5}\text{O}_2$ nanoparticles was investigated. The results showed that the removal rate is very fast (Fig. 9). The decrease in the concentration of RB5 with time is due to the adsorption of RB5 on $\text{LiCo}_{0.5}\text{Fe}_{0.5}\text{O}_2$ nanoparticles.

3.6.3. Effect of adsorbent concentration

Fig. 10 shows the effect of adsorbent dosage of RB5 adsorption by $\text{LiCo}_{0.5}\text{Fe}_{0.5}\text{O}_2$ nanoparticles. Because of increasing the number of binding sites, as the adsorbent dose increases, the percentage removal of dye also goes up.

3.7. Chemical kinetic studies

The first (Eq. (3)) and the second (Eq. (4)) order reaction rate equations are available to investigate the adsorption kinetics [20]. For describing the experimental kinetic, the data fitted to these equations:

$$\ln C(t) = \ln C_0 - k_1 t \quad (3)$$

$$\frac{1}{C(t)} = k_2 t + \frac{1}{C_0} \quad (4)$$

where k_1 and k_2 are the first-order and second-order rate constants, respectively. The plots of experimental results of the two models showed that the removal of dye followed second-order kinetics with a rate constant of $0.002 \text{ M}^{-1} \text{ min}^{-1}$.

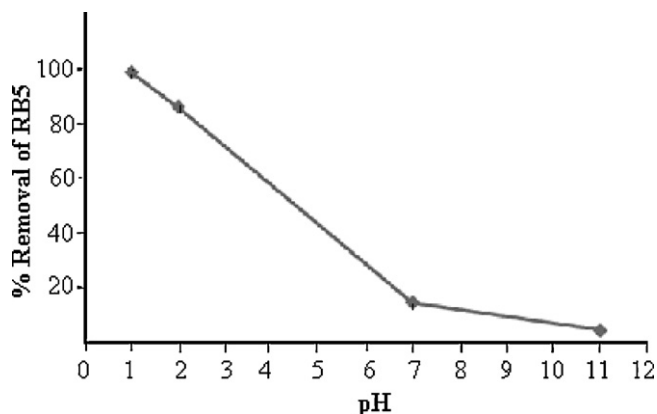


Fig. 8. Effect of pH on RB5 removal by $\text{LiCo}_{0.5}\text{Fe}_{0.5}\text{O}_2$. Experimental conditions: mass of adsorbent, 0.05 g; initial dye concentration, 50 mg l^{-1} ; volume of dye solution, 50 ml; time, 10 min; temperature 25°C .

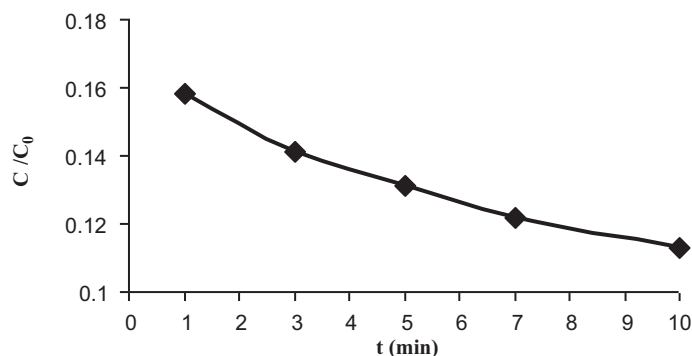


Fig. 9. Removal rate of RB5 on $\text{LiCo}_{0.5}\text{Fe}_{0.5}\text{O}_2$. Experimental conditions: mass of adsorbent, 0.05 g; initial dye concentration, 50 mg l^{-1} ; volume of dye solution, 50 ml; temperature, 25°C ; and $\text{pH} = 1$.

3.8. Adsorption isotherms

Several isotherm models were developed to evaluate the equilibrium adsorption of compounds from solutions such as Langmuir, Freundlich. The experimental results of this study have been fitted with these two models.

The linearized form of the Langmuir isotherm (Eq. (5)), assuming monolayer adsorption on a homogeneous adsorbent surface, is expressed as follows [21]:

$$\frac{C_e}{q_e} = \frac{1}{bq_{\max}} + \frac{C_e}{q_{\max}} \quad (5)$$

where the q_{\max} (mg g^{-1}) is the surface concentration at monolayer coverage which illustrates the maximum value of q_e and it can be attained as C_e is maximized. The b parameter is a coefficient related to the energy of adsorption and increases with increasing strength of the adsorption bond. The values of q_{\max} and b are determined from the linear regression plot of (C_e/q_e) versus C_e . The parameters of the Langmuir equation in this work, namely q_{\max} and b are 76.92 mg g^{-1} and 0.016 L mg^{-1} , respectively (Fig. 11a).

The Freundlich equation (Eq. (6)) [22] is expressed as follows:

$$\log q_e = \log K_F + \frac{1}{n} \log C_e \quad (6)$$

where K_F and n are constants of the Freundlich equation. The constant K_F represents the capacity of the adsorbent for the adsorbate. n is related to the adsorption distribution. A linear regression plot of $\log q_e$ versus $\log C_e$ gives the K_F and n values [23]. The value of correlation coefficient (R^2) for Freundlich isotherm is greater than that of the Langmuir isotherm for the adsorption of the dye (Fig. 11b). This indicates that Freundlich model can

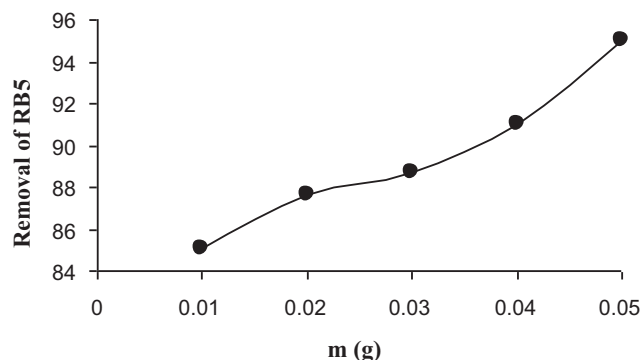


Fig. 10. Effect of adsorbent dosage of RB5 adsorption onto of $\text{LiCo}_{0.5}\text{Fe}_{0.5}\text{O}_2$. Experimental conditions: initial dye concentration, 50 mg l^{-1} ; volume of dye solution, 50 ml; time, 10 min; temperature, 25°C ; and $\text{pH} = 1$.

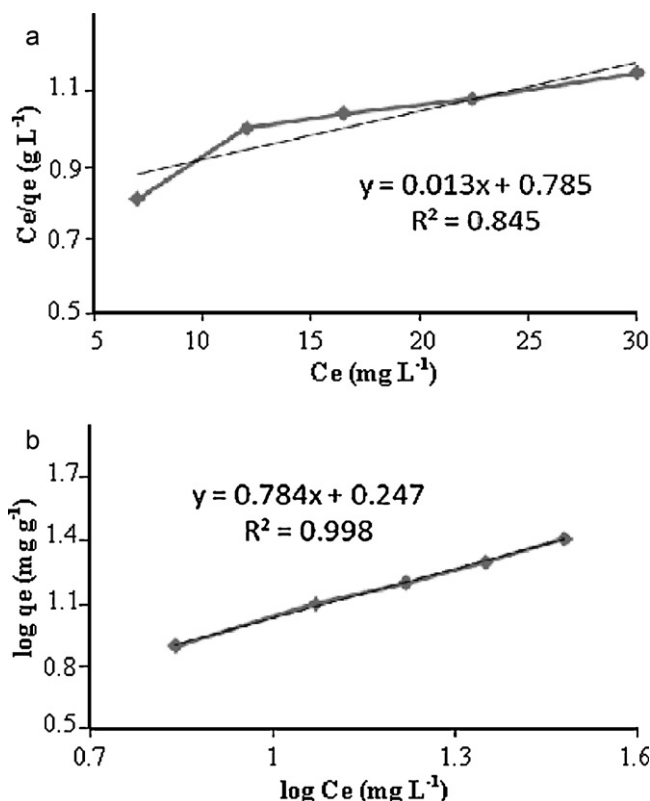


Fig. 11. The plot of linearized form of (a) the Langmuir isotherm, (b) the Freundlich isotherm. Experimental conditions: mass of adsorbent, 0.05 g; initial dye concentration, 50, 75, 100, 150, 200 mg l⁻¹; volume of dye solution, 50 ml; temperature, 25 °C; and pH = 1.

describe the adsorption of RB5 on LiCo_{0.5}Fe_{0.5}O₂ nanoparticles better than the Langmuir model.

3.9. Desorption studies

Desorption studies are important since they contribute to elucidate the nature of adsorption process and adsorbent regeneration. The calculated desorption efficiency are given in Table 2. For repeated use of an adsorbent, adsorbed dye should be easily desorbed under suitable conditions. Desorption process was conducted by mixing 0.05 g of RB5 loaded LiCo_{0.5}Fe_{0.5}O₂ with 25 ml of different concentration of NaOH solutions and shaking for

1 h. It was found that desorption of RB5 from loaded nanoparticles started at pH = 8.

The desorption efficiency calculated as:

$$\text{Desorption (\%)} = \frac{\text{amount of desorbed RB5}}{\text{amount of adsorbed RB5}} \times 100 \quad (7)$$

The RB5 could be desorbed from the loaded nanoparticles by higher concentration of NaOH.

3.10. Performance evaluation

The adsorption capacity varies and it depends on the characteristics of the individual adsorbent and initial concentration of the adsorbate. The maximum adsorption capacity (q_{max}) of LiCo_{0.5}Fe_{0.5}O₂ for RB5 calculated from the Langmuir isotherm model and other adsorbents for organic dyes adsorption are listed in Table 3. It shows that q_{max} of RB5 on LiCo_{0.5}Fe_{0.5}O₂ in this work is high. Therefore, it can be concluded that LiCo_{0.5}Fe_{0.5}O₂ is a fine adsorbent with good adsorption capacity.

4. Conclusions

Nanoparticles LiCo_{0.5}Fe_{0.5}O₂, were prepared using sol gel method in the presence of maleic acid as a chelating agent. The XRD and TEM reveal that the LiCo_{0.5}Fe_{0.5}O₂ nanoparticles prepared by calcinating the gel precursor at 600 °C have good crystallinity with fine rhombohedral delafossite structure. The adsorption studies were carried out for different contact time, pH and adsorbent doses. Also, nanoparticles LiCo_{0.5}Fe_{0.5}O₂, were proven to removal dye RB5 at pH = 1 effectively. The results showed the LiCo_{0.5}Fe_{0.5}O₂ nanoparticles can effectively remove high concentrations of RB5 dye molecules. The second-order kinetic model is more successful in representing the experimental data for the removal of RB5 on LiCo_{0.5}Fe_{0.5}O₂ nanoparticles. The isotherm

Table 2
Desorption of RB5 from nanoparticles LiCo_{0.5}Fe_{0.5}O₂.

Concentration of NaOH (M)	Desorption (%)
0.1	14.76
0.2	19.02
0.3	21.15
0.4	27.69
0.5	30.33

Table 3
Adsorption capacities of organic dyes on various adsorbents.

Adsorbents	Dyes	q_{max} (mg g ⁻¹)	References
ZnCr ₂ O ₄	Reactive blue 5 (RB5)	41.32	[11]
MnFe ₂ O ₄	Methylene blue	20.67	[24]
CuFe ₂ O ₄	Acid red B (ARB)	86.81	[25]
La _{0.5} Ca _{0.5} NiO ₃	Reactive blue 5 (RB5)	36.23	[13]
LiCo _{0.5} Fe _{0.5} O ₂	Reactive blue 5 (RB5)	76.92	Present study
Fe ₃ O ₄	Congo red	68.50	[26]
Rice bran	Congo red	14.60	[27]

evaluations revealed that the adsorption of RB5 by the nanoparticles follows the Freundlich model. Based on the adsorption kinetics and experimental results, we inferred that electrostatic absorption was the main adsorption mechanism.

Acknowledgments

The authors acknowledge the support of the Islamic Azad University, Qeshm Branch, Qeshm, Iran and Ferdowsi University of Mashhad, Mashhad, Iran, for this project (*P*- 47).

References

- [1] M.A. Brown, S.C. De Vito, *Crit. Rev. Environ. Sci. Technol.* 23 (1993) 249–324.
- [2] Y.P. Chang, C.L. Ren, Q. Yang, Z.Y. Zhang, L.J. Dong, X.G. Chen, D.S. Xue, *Appl. Surf. Sci.* 257 (2011) 8610–8616.
- [3] E.N. El Qada, S.J. Allen, G.M. Walker, *Chem. Eng. J.* 135 (2008) 174–184.
- [4] A.L. Ahmad, S.W. Puasa, *Chem. Eng. J.* 132 (2007) 257–265.
- [5] J. Labanda, J. Sabate, J. Llorens, *J. Membr. Sci.* 340 (2009) 234–240.
- [6] M.E. Osugi, K. Rajeshwar, E.R.A. Ferraz, D.P. de Oliveira, R. Arojo, M.V.B. Zanoni, *Electrochim. Acta* 54 (2009) 2086–2093.
- [7] A.R. Tehrani-Bagha, N.M. Mahmoodi, F.M. Menger, *Desalination* 260 (2010) 34–38.
- [8] G. Mezohegyi, F. Goncalves, J.J.M. Orfao, A. Fabregat, A. Fortuny, J. Font, C. Bengoa, F. Stuber, *Appl. Catal. B: Environ.* 94 (2010) 179–185.
- [9] A.N. Chowdhury, A. Rahim, Y.J. Ferdosi, Md S. Azam, M.M. Hossain, *Appl. Surf. Sci.* 256 (2010) 3718–3724.
- [10] M.A. Marquardt, N.A. Ashmore, D.P. Cann, *Thin Solid Film* 496 (2006) 146–156.
- [11] M. Yazdanbakhsh, I. Khosravi, E.K. Goharshadi, A. Youssefi, *J. Hazard. Mater.* 184 (2010) 684–689.
- [12] I. Khosravi, M. Yazdanbakhsh, E.K. Goharshadi, A. Youssefi, *Mater. Chem. Phys.* 130 (2011) 1156–1161.
- [13] M. Yazdanbakhsh, H. Tavakkoli, S.M. Hosseini, *Desalination* 281 (2011) 388–395.
- [14] C. Julien, *J. Solid State Ionics*. 136 (2000) 887–896.
- [15] D.M. Indra, C.S. Vimal, K.A. Nitin, *Dyes Pigments* 69 (2006) 210–223.
- [16] Y. Shifeng, Y. Jingbo, Z. Enle, *J. Alloy. Compd.* 450 (2008) 417–420.
- [17] G. Bayramoglu, G. Celik, M.Y. Arica, *J. Hazard. Mater. B.* 137 (2006) 1689–1697.
- [18] H.E. Zhang, B.F. Zhang, G.F. Wang, X.H. Dong, Y. Gao, *J. Magn. Magn. Mater.* 312 (2007) 126–130.
- [19] A.K. Bhattacharya, T.K. Naiya, S.N. Mandal, S.K. Das, *Chem. Eng. J.* 137 (2008) 529–541.
- [20] S.C.R. Santos, V.J.P. Vilar, R.A.R. Boaventura, *J. Hazard. Mater.* 153 (2008) 999–1008.
- [21] I. Langmuir, *J. Am. Chem. Soc.* 40 (1918) 1361–1403.
- [22] H.M.F. Freundlich, *Phys. Chem. A.* 57 (1906) 385–471.
- [23] B. Singha, S.K. Das, *Colloids Surf. B: Biointerfaces* 84 (2011) 221–232.
- [24] X.Y. Hou, J. Feng, Y.M. Ren, Z.J. Fan, M.L. Zhang, *Colloids Surf. A: Physicochem. Eng.* 363 (2010) 1–7.
- [25] R.C. Wu, J.H. Qu, H. He, *Appl. Catal. B.* 48 (2004) 49–56.
- [26] L. Wang, J. Li, Y. Wang, L. Zhao, Q. Jiang, *Chem. Eng. J.* 182 (2012) 72–79.
- [27] X.S. Wang, J.P. Chen, *Sep. Sci. Technol.* 44 (2009) 1452–1466.